Bistability of orthotropic shells with clamped boundary conditions: An analysis by the polar method

Matteo Brunetti, Stefano Vidoli, Angela Vincenti

Bistability of orthotropic shells with clamped boundary conditions: an analysis by the polar method

Matteo Brunetti[a,*], Stefano Vidoli[a], Angela Vincenti[b]

[a]*Dipartimento di Ingegneria Strutturale e Geotecnica, Sapienza Università di Roma, via Eudossiana 18, 00184, Rome, Italy*

[b]*Institut Jean Le Rond d'Alembert, Sorbonne Universities, UPMC Univ Paris 06, CNRS, UMR 7190, 75005, Paris France*

Abstract

Multistable shells have been recently proposed as an effective solution to design morphing structures. We describe a class of shallow shells which are bistable after one of their sides, initially curved, is clamped along a flat line. Supposing the shell being assembled as a composite laminate, we show how the anisotropy of the material can influence the multistable behaviour and the robustness of stable configurations. Specifically, we focus on orthotropic laminated shells using the polar method for a complete representation of the anisotropic elastic properties. Two experimental prototypes have been produced and tested to validate our analytical and numerical results.

Keywords: Morphing Structures, Multistability, Polar method, Orthotropy.

1. Introduction

One of the emerging challenges in structural engineering is to design structures able to face quite different operating conditions. This goal can be achieved by resorting to morphing structures *i.e.* structures capable of updating their geometric configuration in order to satisfy some performance requirements. Even if morphing structures are becoming more widespread in some areas of structural engineering (see [5, 16]), much remains to be done to properly design and implement this kind of systems.

Morphing structures can be realized by means of multistable shells, *i.e* elastic surfaces that exhibit more than one equilibrium configuration. These configurations can then be maintained without applying external actions. Since actuation is required only to switch between the alternative stable states and it could be realized with a limited actuation force (*e.g.* by triggering instability phenomena, or by exploiting displacement amplifications due to geometrical nonlinearities), multistable shells turn out to be a cheap way to get structural systems capable of considerable shape change.

Multistability in shells stems from a complex interplay between geometric nonlinearities and elastic properties, and it can be achieved in various ways combining initial natural curvatures of the shell and curvatures induced by pre-stresses (such as plastic deformations or multi-physical couplings [11]). Moreover, multistability is highly sensitive to boundary conditions and the anisotropy of the constitutive material can play an important role [23]. The global stability scenario, the number of the stable equilibrium configurations, their shapes and their 'robustness', depends on such choices and should be completely known to properly design the morphing system. However stable states usually have quite different shapes and the transition

*Corresponding author

Email addresses: matteo.brunetti@uniroma1.it (Matteo Brunetti), stefano.vidoli@uniroma1.it (Stefano Vidoli), angela.vincenti@upmc.fr (Angela Vincenti)

between them may be realized by following different load paths: in this sense, finite-element analysis serves little purpose to depict such global stability scenario, whilst *reduced* shell models with few degrees of freedom are much more useful.

For shallow shells, as the ones commonly used in technological applications, the nonlinear (generalized) von Kármán shell model [25] can be chosen as 'parent' model. Then, the discrete model can be generated by reducing the parent model to a low-dimensional subspace by means of a careful selection of admissible configurations. Indeed, an effective reduction should globally preserve the multi-well elastic energy of the parent model, see [17, 23, 24].

Despite the relevance of boundary conditions, most of the literature studies deal with shells completely free on their sides, see for instance [4, 6, 7, 13, 15, 17, 23], and only few address the design of multistable constrained shells [8, 14]. In [1] the authors used the reduction procedure proposed in [24] to infer a three-degrees-of-freedom reduced model capable of predicting the multistable behavior of pseudo-conical cantilever orthotropic shells. They identified two compact disjoint regions in the plane of shell initial curvatures corresponding to bistable shells *after clamping*, thus opening the way to a more general approach to the design and optimization of multistable shells.

In the present work, we consider the initial geometry of the natural stress-free configuration and the elastic properties of the shell as the only means to induce bistability, excluding other sources of multistability such as inelastic pre-stresses. We use the same model as in [1] to investigate how the material anisotropic elastic properties affect the multistability of clamped shells.

Specifically we tailor the anisotropic elastic behaviour of the constitutive material of the shell using composite laminates, where the combination of ply angles in a layup allows to cover a wide range of elastic parameters and anisotropic behaviours. In order to better understand the influence of anisotropy, we employ the *polar method* [22, 20] which makes it possible to express tensors in plane elasticity in terms of invariant quantities. For an orthotropic laminate with a given base ply material, one can describe the elastic properties in terms of only three polar parameters, two invariants elastic moduli and an angle that represents the direction of the principal orthotropy axis. As such, the polar method allows to clearly highlight the influence of the anisotropic behaviour of laminates on the multistability scenarios.

For sake of simplicity, we choose two initial geometries for the shell natural configuration and we consider uncoupled quasi-homogeneous orthotropic laminates [19]. We detect the regions in the plane of the polar moduli corresponding to shells which turn out to be bistable after clamping; moreover, we investigate the influence of the polar moduli on the shapes of the clamped stable configurations and on the energetic gap between them. In that, we take advantage of the polar method to provide some insights about the role of the lamination sequences; specifically, for angle-ply laminates we point out the influence of the lamination angle. Such informations are deemed to be very useful in the early stages of the design of morphing shells.

The paper is organized as follows. Section 2 introduces the relevant geometric properties of the shells and the polar method notation for the material moduli. Section 3 presents the main results: mono- and bistability regions are shown on the plane of polar moduli. We sketch the shell stable shapes for several special choices of the material anisotropy and discuss the associated elastic energy profiles. Finally we compare such results with the experimental evidence of two composite laminated shells. The main hypotheses of the reduced shell model and the procedure used to estimate the minimal energy gap between different equilibria are discussed in two Appendices.

2. Geometric and material parameters

2.1. Geometry of the shell natural shapes

We consider shallow shells with rectangular planform and pseudo-conic natural configurations, which can be described by surfaces in the form:

$$\mathcal{S}_0 = \{(x, y, w_0(x, y)),\ 0 \leq x \leq L_x,\ -L_y/2 \leq y \leq L_y/2\},$$

with:

$$w_0(x, y) = \frac{y^2}{2}\left(h_1 + (h_2 - h_1)\frac{x}{L_x}\right), \tag{1}$$

for some $h_1, h_2 \in \mathbb{R}$ and $0 < L_y \leq L_x$. The geometry of the natural configuration of the shell is completely defined by three design parameters: the aspect ratio of the planform $\eta = L_x/L_y \geq 1$ and the real numbers h_1 and h_2, which measure the curvatures of the edges parallel to the y-direction $x = 0$ and $x = L_x$, respectively. This class of natural configurations has been chosen because it is sufficiently wide to include shapes suitable for technogical applications and simple enough to allow a proper understanding of the role played by the parameters it depends on.

In what follows only two natural configurations will be considered. The first, displayed in Fig. 1a, has curvatures h_1 and h_2 concordant in sign and will be labeled as (CC); the second, sketched in Fig. 1b has discordant edge curvatures and will be labeled as (DC).

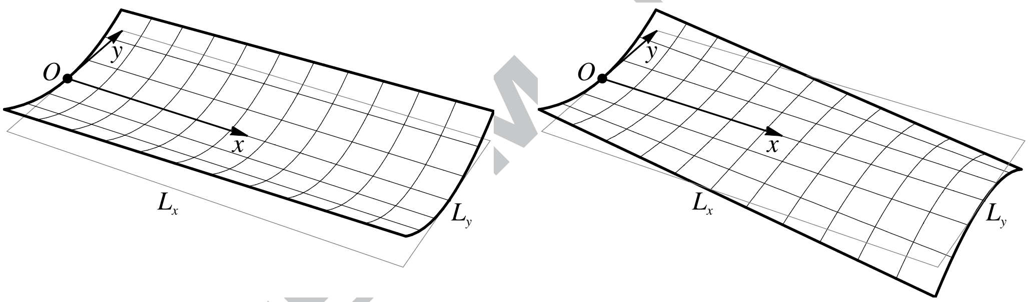

(a) CC (b) DC

Figure 1: The two natural configurations considered: shells with Concordant (a) and Discordant (b) Curvatures of the opposites edges.

The values chosen for the geometrical design parameters L_x, L_y, h_1 and h_2 are listed in Table 1. In order for the shell to be thin, edges lengths L_x, L_y have been chosen sufficiently large compared to the laminate thickness t, here equal to 1 mm; their ratio L_x/L_y allows to have a bistability region wide enough for both (CC) and (DC) cases, see [1]. The curvatures h_1, h_2 have been chosen so that the shallowness ratio $w_{\max}/L_y$ is 1/8 for the edge $x = 0$ (this is the edge to be clamped), and 1/6 for the edge $x = L_x$ (to be left free). Both geometries in Table 1 share the same aspect ratio $\eta = 2$ and only differ by the sign of the curvature of the free edge. As the difference of the curvature radii is small compared to the length, $|h_1^{-1} - h_2^{-1}|/L_x \simeq 0.125$, the CC shell is quasi-cylindrical.

Table 1: Geometric design parameters

	L_x (m)	L_y (m)	h_1 (1/m)	h_2 (1/m)	t (m)
Concordant Curvatures (CC)	0.3	0.15	1/0.15	1/0.1125	0.001
Discordant Curvatures (DC)	0.3	0.15	1/0.15	-1/0.1125	0.001

The same natural configurations were already studied in [1] and it was shown that bistability can be obtained by clamping these two shells along their curved side $x = 0$ onto a flat line in a wide range of values for the geometric parameters η, h_1 and h_2. However, the analysis in [1] was conducted with fixed material properties; in particular, the authors considered shells made of an uncoupled square-symmetric $\pm 45°$ angle-ply laminate. In the present work, we keep the geometries of the natural configurations fixed and focus on the influence of composite anisotropic behaviour on the multistability scenario.

2.2. Material constants of a composite laminated shell

As the shells under consideration are sufficiently thin and shallow we adopt the Föppl von-Kármán model [25, 3] to compute their equilibria and stability (see Appendix A). Within this model the material is assigned by the following linear constitutive prescriptions

$$\boldsymbol{n} = \boldsymbol{A}\,(\boldsymbol{e} - \boldsymbol{f}) + \boldsymbol{B}\,(\boldsymbol{k} - \boldsymbol{h})\,, \qquad \boldsymbol{m} = \boldsymbol{D}\,(\boldsymbol{k} - \boldsymbol{h}) + \boldsymbol{B}^{\top}\,(\boldsymbol{e} - \boldsymbol{f})\,, \tag{2}$$

relating the membrane stresses and bending moments to the membrane strains and to the curvatures. In particular we have used the Voigt notation to indicate:

- the membrane stresses $\boldsymbol{n} = \{n_x, n_y, n_s\}$ ($n_s = n_{xy}$ is the shear component);
- the bending moments $\boldsymbol{m} = \{m_x, m_y, m_s\}$ ($m_s = m_{xy}$ is the twisting component);
- the membrane strains $\boldsymbol{e} = \{e_x, e_y, e_s\}$ ($e_s = 2e_{xy}$ is the shear strain)
- the curvatures $\boldsymbol{k} = \{k_x, k_y, k_s\}$ ($k_s = 2k_{xy}$ is the twisting curvature);

In order to account for a curved natural (*i.e* stress-free) configuration, we have also introduced the strains $\boldsymbol{f} = \{f_x, f_y, f_s\}$ and curvatures $\boldsymbol{h} = \{h_x, h_y, h_s\}$ of the natural configuration. Clearly these must obey the Gauss compatibility equation

$$\frac{\partial^2 f_x}{\partial y^2} + \frac{\partial^2 f_y}{\partial x^2} - 2\frac{\partial^2 f_{xy}}{\partial x \partial y} = h_x h_y - h_{xy}^2. \tag{3}$$

The three 3×3 matrices $\boldsymbol{A}$, $\boldsymbol{B}$ and $\boldsymbol{D}$ in (2) indicate the membrane, coupling and bending stiffnesses respectively. In order to give a synthetic analysis of the multistability behaviour of orthotropic shells, we suppose the constitutive material of the shell to be uncoupled and to have the same elastic behaviour in tension and bending in each direction. In the language of Classical Laminated Plate Theory [2, 19], we suppose the material to be quasi-homogeneous and orthotropic with principal directions aligned with the coordinate directions x and y. These assumptions imply

$$\boldsymbol{A} = t\,\boldsymbol{A}^*, \quad \boldsymbol{B} = \boldsymbol{0}, \quad \boldsymbol{D} = \frac{t^3}{12}\,\boldsymbol{A}^*, \quad \boldsymbol{A}^* = \frac{a}{t}\begin{bmatrix} 1 & \nu & 0 \\ \nu & \beta & 0 \\ 0 & 0 & \gamma \end{bmatrix}, \tag{4}$$

where t is the equivalent shell thickness and $\boldsymbol{A}^*$ the normalized membrane stiffness. As the membrane and bending stiffness are mutually proportional, only four constitutive parameters are sufficient to fix the shell material properties. Specifically, a measures the membrane and bending stiffness in the x direction, β controls the ratio between the membrane and bending stiffnesses in the two coordinate directions, ν measures the in-plane and out-of-plane Poisson effects and γ controls the shear and torsional moduli.

Since composite laminates are an effective means to tailor anisotropic stiffness, we consider that the aforementioned material properties are achieved by using laminates and adopt the polar method [22, 20] to represent the normalized stiffness tensor $\boldsymbol{A}^*$. Within this representation, four material invariants T_0, T_1, R_K and R_1 and one angle $\varPhi_1$ are sufficient to describe the orthotropic stiffness tensors of a quasi-homogeneous laminate [12]. Namely, we have

$$\begin{aligned} a/t &= \quad T_0 + 2T_1 \quad + R_K \cos 4\varPhi_1 + 4R_1 \cos 2\varPhi_1, && (5)\\ a\,\beta/t &= \quad T_0 + 2T_1 \quad + R_K \cos 4\varPhi_1 - 4R_1 \cos 2\varPhi_1, && (6)\\ a\,\nu/t &= -T_0 + 2T_1 \quad - R_K \cos 4\varPhi_1, && (7)\\ a\,\gamma/t &= \qquad T_0 \qquad - R_K \cos 4\varPhi_1, && (8) \end{aligned}$$

where T_0 and T_1 are positive scalars representing the isotropic components of the tensor, whilst the anisotropic components are R_K and R_1: R_K is a real number (positive or negative values of R_K respectively correspond to low- or high-shear orthotropic materials [20]) and R_1 is a non-negative modulus. Finally, the angle $\varPhi_1$ identifies the principal direction of orthotropy of the laminate; in our case, the condition for the principal orthotropy direction to be aligned with either x- or y-direction implies $\varPhi_1 = 0°$ or $\varPhi_1 = 90°$, respectively. Correspondingly, one can notice that in expressions (5) $\cos 2\varPhi_1 = \pm 1$, whilst $\cos 4\varPhi_1 = 1$ in both cases.

The advantage of this representation is that for laminates made of identical layers (same base material and same thickness), it can be easily shown that the isotropic components of the normalized stiffess tensor $\boldsymbol{A}^*$ are equal and coincide to those of the elementary layer, say T_0^ℓ and T_1^ℓ [12]. Thus, using the polar method, only the two anisotropic parameters R_K and R_1 are left to represent the elastic behaviour of uncoupled quasi-homogeneous orthotropic laminates. Hence, after choosing the elementary layer, the admissible domain of uncoupled orthotropic laminates reduces to a two-dimensional region within the R_K-R_1 plane.

In particular, the admissible values of the anisotropic parameters of the tensor $\boldsymbol{A}^*$ are bounded because they depend on the combination of layers' orientation angles within the laminate stacking sequence, [12, 21]. Using the superscript ℓ for the polar parameters of the elementary layer, these bounds are:

$$R_K \geq R_K^\ell \left[2 \left(\frac{R_1}{R_1^\ell} \right)^2 - 1 \right], \tag{9a}$$

$$-R_K^\ell \leq R_K \leq R_K^\ell, \tag{9b}$$

$$0 \leq R_1 \leq R_1^\ell. \tag{9c}$$

Points satisfying the bounds (9) are represented by the upper half of the grey domain in Figure 2 (*i.e.* non-negative values of R_1, according to (9c)). Since $\varPhi_1 = 0, \pi/2$ corresponds to the quantity $R_1 \cos 2\varPhi_1 = \pm R_1$, we can identify the upper half of the domain ($R_1 > 0$) to the case of an orthotropic laminate with the principal orthotropy direction aligned with axis x (case $\varPhi_1 = 0$). Each point of the upper half of the domain has a symmetric counterpart in the lower half (negative R_1): the symmetric point represents the same laminate configuration (same elastic moduli) shifted by 90°, *i.e.* with principal orthotropy direction aligned with the y axis (case $\varPhi_1 = \pi/2$). Thus, the complete domain of orthotropic quasi-homogeneous laminates with their principal orthotropy axes aligned with either the x- or y-axis of the plate is shown by the grey region in Figure 2.

Points on the curved boundary A-B-C correspond to orthotropic *angle-ply* laminates, *i.e.* laminates with equal number of layers at angles α and $-\alpha$. Moving from point A to C, the lamination angle varies from $\alpha = 0°$ to $\alpha = 90°$: points A and C represent unidirectional laminates with fibers aligned along the x- or y-direction, respectively. Point B corresponds to the square-symmetric angle-ply laminate with $\alpha = 45°$, which was studied in [1] and used in [4] to build a tristable shell. Points on the right boundary of the domain (segment A-D-C) correspond to *cross-ply* laminates, with layers oriented at angles 0° and 90° in varying proportion: in particular, point D can be achieved with an equal number of layers at each orientation

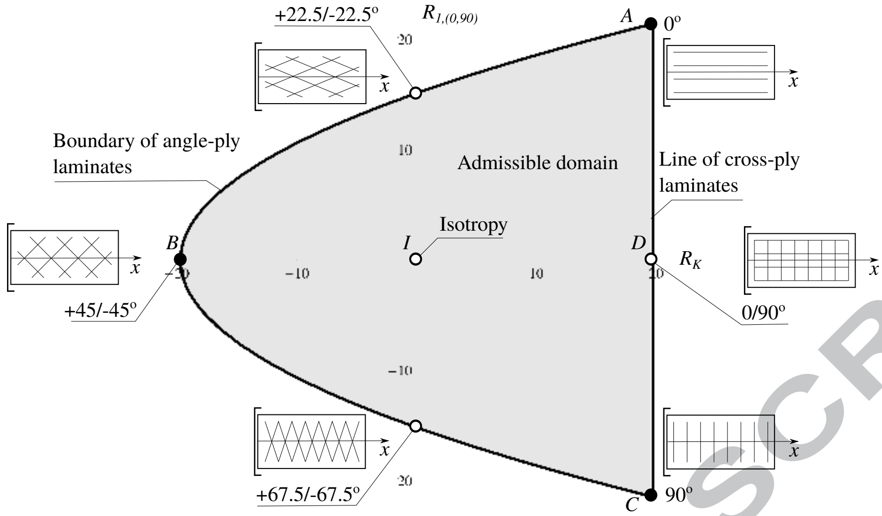

Figure 2: Admissible domain in the plane of the polar parameters R_K and R_1. Numerical values are in GPa and correspond to the base material in Table 2.

in the stacking sequence. Points on the horizontal axis $R_1 = 0$ represent square-symmetric laminates, whilst points on the vertical axis $R_K = 0$ own a special form of orthotropy, see [19], characterised by a constant value of the shear or torsional modulus. Finally, the origin of the R_K-R_1 plane represents an isotropic laminate.

3. Multistable scenario as function of the polar parameters

We choose the polar moduli R_K and R_1 as the only design parameters. In particular, we fix the material parameters for the elementary layer; hence, for both the shell natural configurations of Figure 1, we determine the regions in the plane R_K-R_1 corresponding to bistable shells after clamping.

Table 2: Material properties of the unidirectional carbon/epoxy ply TenCate TC275-1 Epoxy Resin System (Grafil TR50S 15K fiber with a FAW 150 gsm, 35% RC). Values from the product data sheet [27].

E_1	E_2	ν_{12}	G_{12}	T_0^ℓ	T_1^ℓ	R_K^ℓ	R_1^ℓ
GPa	GPa	-	GPa	GPa	GPa	GPa	GPa
152.4	10.3	0.3	3.4	21.4	21.2	17.9	17.8

A highly anisotropic unidirectional carbon/epoxy ply has been chosen, the overall thickness of the shell being fixed at $t = 1$ mm, see Table 2. This latter assumption implies a laminate made by $N = 8$ layers, which is the minimal condition for designing uncoupled quasi-homogeneous orthotropic laminates. Specifically, we can easily cover the curved boundary A-B-C of the admissible domain in Figure 2 using the exact solution provided by [19] for the 8-layer angle-ply antisymmetric stacking sequence:

$$[\alpha/-\alpha/-\alpha/\alpha/-\alpha/\alpha/\alpha/-\alpha]\,, \quad \text{with: } \alpha \in [0^\circ, 90^\circ]. \tag{10}$$

Other points of the domain of orthotropic laminates of Fig. 2 correspond to different stacking sequences that can be determined by applying an optimisation approach such as in [10].

In the present work, for both the natural configurations and for each choice of the moduli R_K-R_1 within the admissible domain of Fig. 2, we use the reduced model of Föppl von-Kármán shallow shell detailed in Appendix A to predict the number of stable configurations as well as their shapes. When the shell is bistable, we compute the minimal energy path between the two wells using the algorithm detailed in Appendix B.

3.1. Mono- and bistability regions

Fig. 3 displays the global stability scenario over the admissible domain in the plane of the polar moduli R_K-R_1. The grey and white regions correspond, respectively, to shells that are *bistable* and *monostable* after clamping the edge $x = 0$.

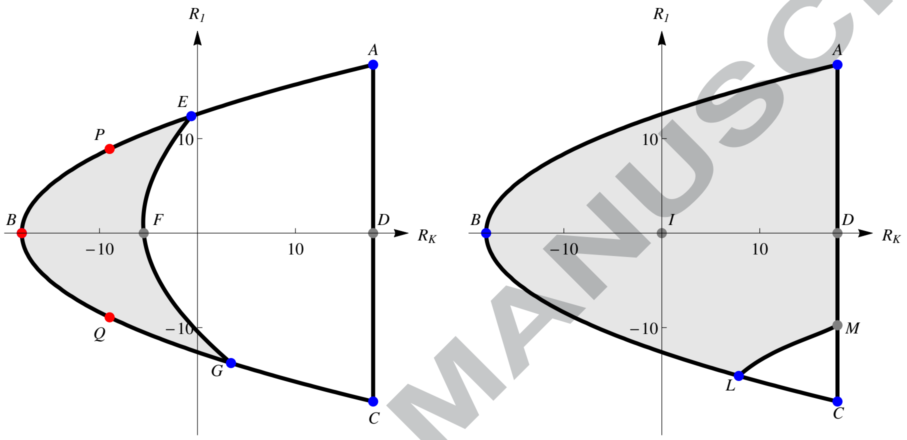

(a) Concordant Curvatures shell (CC). (b) Discordant Curvatures shell (DC).

Figure 3: Stability scenario in the plane of polar moduli.

The bistable region of shells with Concordant Curvatures (CC) of their opposite sides is sensibly smaller, see Fig. 3a. As already pointed out in [1], these shells exhibit quasi-cylindrical configurations with small stability margins. Specifically, the existence of bistable shells is mostly limited to negative values of R_K, *i.e.* high-shear orthotropic laminates (refer to (8)). This region spans almost symmetrically with respect to the horizontal axis ($R_1 = 0$). Hence, bistability is obtained either by aligning the principal axis of orthotropy to the longitudinal x axis ($R_1 > 0$) or to the transverse y axis ($R_1 < 0$). The bistability region borders are the arc E-B-G on the left, corresponding to angle-ply laminates with angles $\alpha \in [24°, 70°]$ approximatively, and the arc E-F-G on the right, with $F = (R_K \approx -5.8 \text{ GPa}, R_1 = 0)$. In particular, one can see that the CC shell made of isotropic laminates ($R_K = 0, R_1 = 0$) is not bistable.

In the case of shells with Discordant Curvatures (DC) of their opposite sides, bistability is obtained over a much wider set of material parameters. Specifically, the bistable region in Fig. 3b covers almost the whole admissible domain of orthotropic laminates: only shells close to the corner of unidirectional laminates in the transverse direction ($\alpha \simeq 90°$) are, indeed, monostable. The bistability region is limited on the left by the A-B-L arc, *i.e.* all angle-ply laminates with $\alpha \in [0°, 73°]$, and on the right by the segment A-D-M which corresponds to cross-ply laminates (*i.e.* $R_K = R_K^\ell = 17.9$ GPa); the limit point M stands for a cross-ply layup with $R_1 \approx 9.8$ GPa and the main direction of orthotropy Φ_1 shifted at 90° with respect to the x-axis. Notice that the isotropic laminate, *i.e.* point I in Fig. 3b, is now included within the bistability domain.

3.2. Configurations and energy profiles for (CC) shells

With reference to the CC shell, we analyse how the shapes of bistable configurations evolve over the bistability domains of Fig. 3a. To give a synthetic quantitative description of these shapes, we compute the curvatures

$$K_x = \frac{1}{L_x}\int_0^{L_x} k_x(x,0)\,dx, \qquad K_y = \frac{1}{L_y}\int_{-L_y/2}^{L_y/2} k_y(L_x,y)\,dy, \tag{11}$$

respectively meaning the average k_x curvature of the shell axis ($y = 0$) and the average k_y curvature of the free edge $x = L_x$. In addition, for each pair of stable configurations, we compute the energy profile according to the procedure described in Appendix B. The results are given in Fig. 4. In particular, Fig. 4a reports the variations of the average curvatures for the main points highlighted in Fig. 3a, Fig. 4b and Fig. 4c plot the actual (*i.e.*, not scaled, nor magnified) shapes and the energy profiles for three angle-ply laminates corresponding to points P, B and Q in Fig. 3a.

The main results shown in Fig. 4 are summarized in the following.

There are two disconnected equilibrium branches; on both, the stable shapes are characterised by positive curvatures K_x and K_y.

The first branch, identified by a subscript 1, is stable on the whole domain. It is characterized by a small value of the average axial curvature $RK_x \leq 3$ and by values of the average edge curvature within $4 \leq RK_y \leq 8$ (R is here the characteristic radius of curvature of the shell, see Appendix A). For angle-ply laminates, as the angle α varies from 0° to 90°, the point representative of the material properties moves on the arc $A - E - B - G - C$ and the equilibrium follows the curve $A_1 - E_1 - B_1 - G_1 - C_1$. Along this path there is a substantial increase of the curvature K_y mainly due to a decreasing value of the $D_{yy} = t^2 a\,\beta/12$ stiffness. Similarly if the material point is moved along the line $B - F - D$ ($R_K = 0$), the curvature K_x remains almost constant along the path $B_1 - F_1 - D_1$ but the free edge curvature increase.

The second branch, identified by a subscript 2, is stable only in the bistability region (light grey area). These equilibria are characterized by vanishing values of the edge curvature K_y, whilst the average axial curvature changes from $RK_x \simeq 2$ to $RK_x \simeq 20$. In particular, on the arc $E - B - G$ of angle ply laminates the limit points of the bistable region are E where $\alpha \simeq 24°$ and G where $\alpha \simeq 70°$. Therefore, when $\alpha < 24°$ or $\alpha > 70°$ the second branch looses its stability.

The stable shapes associated at the points P, B and Q are reported in Fig. 4b. As α increases from 30° (point P) to 60° (point Q) it is evident the substantial increase of the axial curvature in the second equilibrium branch.

Fig. 4c reports the energetic profiles of the elastic energy for angly-ply laminates on the arc $E - B - G$, the coordinate s being a normalized abscissa between the minima. As the angle α varies from 24° to 70°, we note a sensible increment of the energy content of both configurations. Indeed, as α increases the transverse stiffness $D_{yy} = t^2 a\,\beta/12$ increases and, in turn, the pre-stress associated to clamping the edge $x = 0$ increases. We could also observe how the stability margin of the second branch becomes vanishing as $\alpha \to 70°$.

3.3. Configurations and energy profiles for (DC) pseudo-conical shells

With reference to the DC shell, we analyse how the shapes of bistable configurations evolve over the bistability domains of Fig. 3b. Again, in order to give a synthetic quantitative description of these shapes, we observe how the average curvatures K_x and K_y vary on the domain of polar moduli. The results are given in Fig. 5 and are summarized in the following.

There are two disconnected equilibrium branches lying in opposite quadrants on the average curvature plane K_x-K_y.

The first branch, identified by a subscript 1, is stable on the whole domain. It is characterized by average curvatures of opposite signs $1 \leq RK_x \leq 2$ and $-8 \leq RK_y \leq -4$ (R is here

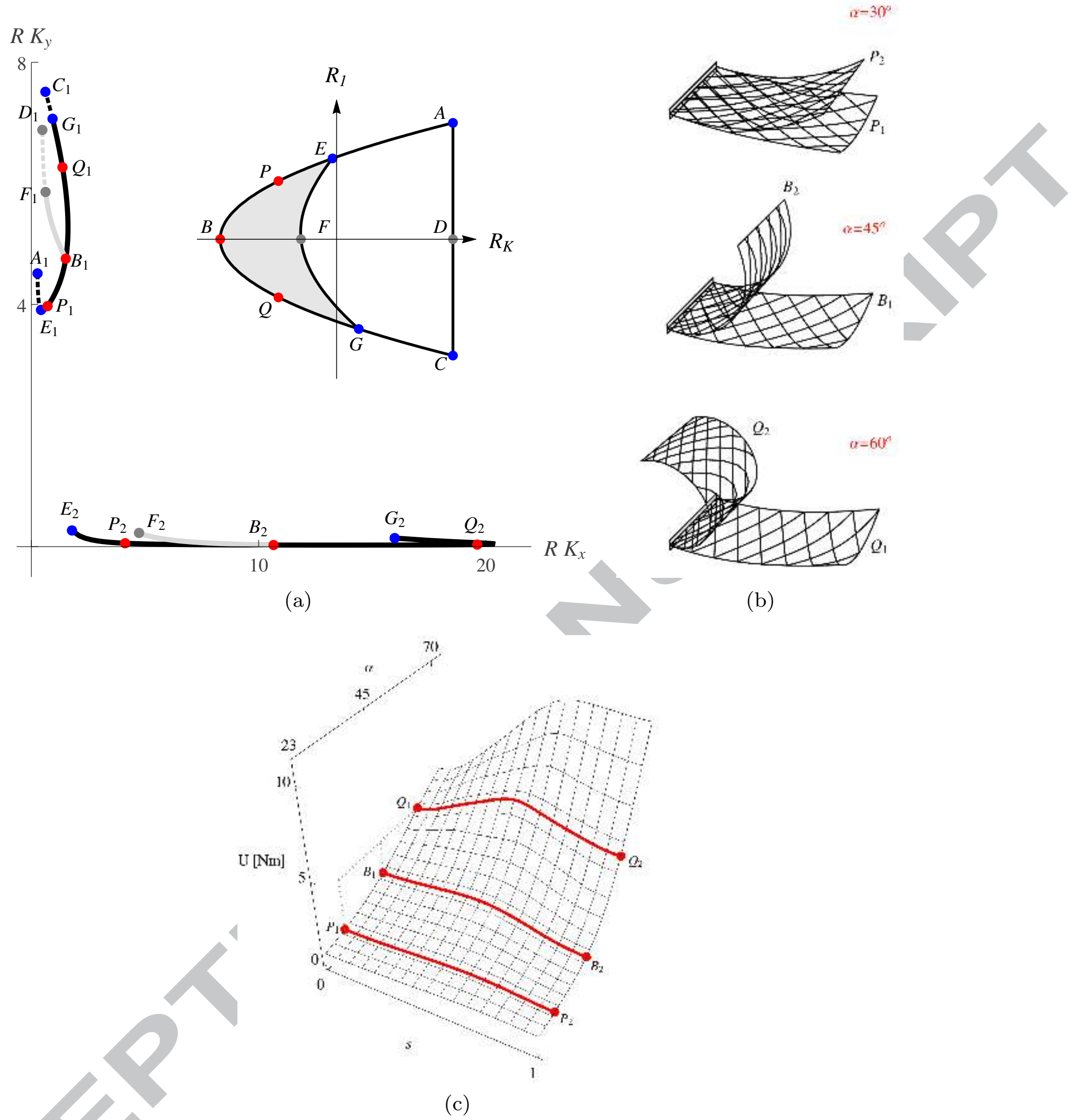

Figure 4: Variation of stable configurations in the admissible domain of Concordant Curvatures shell. (a) Average curvatures K_x and K_y in Eqn. (11); the characteristic curvature radius is set to $R = 1.6\,\mathrm{m}$. (b) Stable shapes for the angle-ply laminates P, B and Q; (c) Elastic energy profiles for the same laminates P, B and Q; s is the normalized abscissa between the minima, see Appendix B.

the characteristic radius of curvature of the shell, see Appendix A). For angle-ply laminates, as the angle α varies from $0°$ to $90°$, the point representative of the material properties moves on the arc $A - B - C$ and the equilibrium follows the curve $A_1 - B_1 - C_1$. Along this path the absolute value of K_y curvature decreases, whilst the axial curvature K_x slightly increases. In any case the shape variations of this equilibrium branch are quite small as can be checked from three shapes L_1, B_1 and A_1 in Fig. 5b.

The second branch, identified by a subscript 2, is stable only in the bistability region (light grey area). These equilibria are characterized by much sharper variations as the material is varied within the $R_1 - R_K$ domain. The second branch becomes unstable when approaching the region near the corner point C, the limit point on the boundary of angle-ply laminates being L where $\alpha \simeq 73°$. In this region the ratio $\beta = D_{yy}/D_{xx}$ between the bending stiffnesses

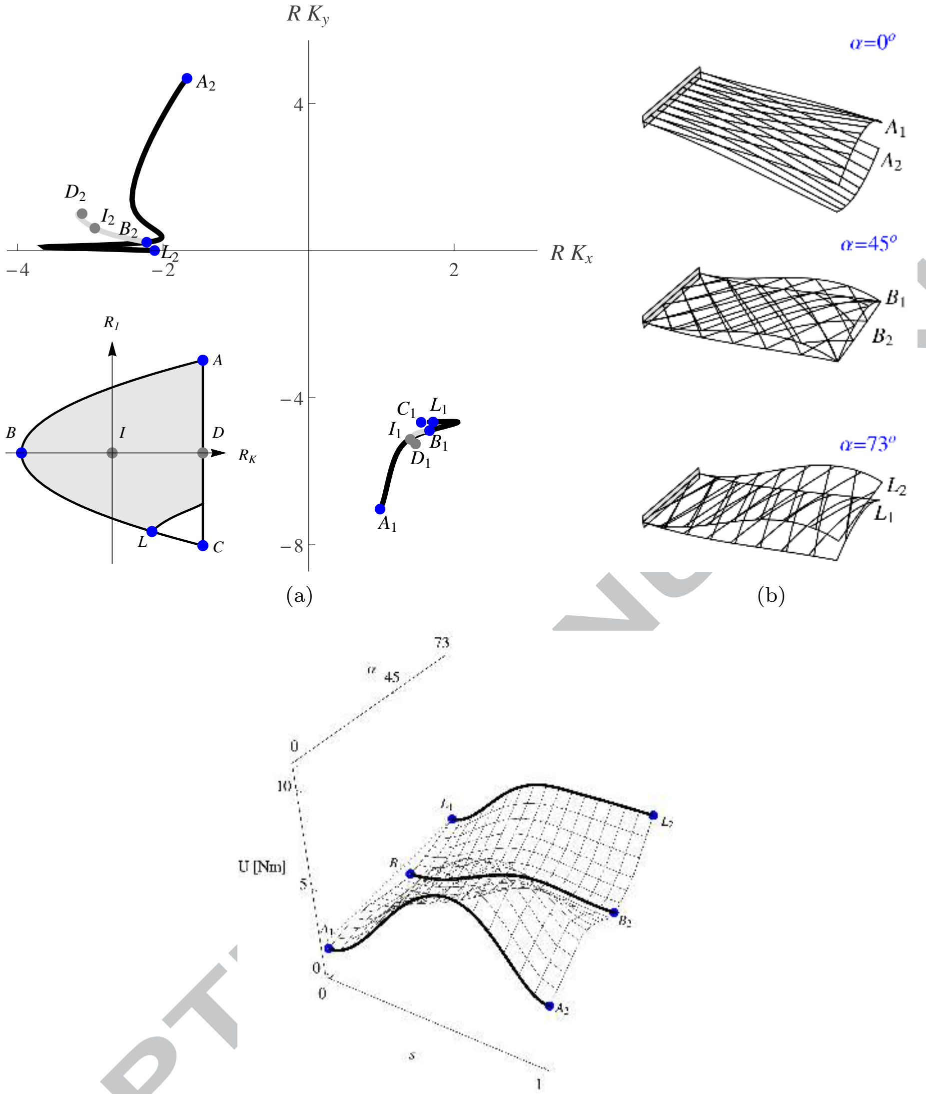

(a) (b)

(c)

Figure 5: Variation of stable configurations in the admissible domain of Discordant Curvatures shell. (a) Average curvatures K_x and K_y in Eqn. (11); the characteristic curvature radius is set to $R = 1.6\,\mathrm{m}$. (b) Stable shapes for the angle-ply laminates A, B and L. (c) Elastic energy profiles for the same laminates A, B and L; s is the normalized abscissa between the minima, see Appendix B.

in the coordinate direction becomes large; $\beta \to 15$ as the material point tends to C.

The stable shapes associated with the material points A, B and L are reported in Fig. 5b, again without scaling or magnification. As α increases from 0° (point A) to 73° (point L) the second branch sensibly changes, passing from the configuration A_2 to the S-shaped configurations B_2 and L_2. We point out that the prediction of the shape B_2, here obtained with the von-Kármán model, was found to be very close with the shape numerically predicted by Abaqus FE using a completely nonlinear shell model, see [1].

Fig. 5c reports the energetic profiles of the elastic energy for angly-ply laminates on the arc $A - B - L$; again, the coordinate s is a normalized abscissa between the minima. We notice that the energetic content of the two configurations is similar and has moderate variations with respect to the angle α. Again one could appreciate the vanishing stability margin of the second branch as $\alpha \to 73°$. We point out that the angle α sensibly affects the energy gap between equilibria; hence we could obtain sensibly different energy profiles of the morphing structure by modest variations of the angle α.

3.4. Comparison with experimental evidence

In cooperation with Aviorec [26], two Concordant Curvature shells have been produced corresponding to the material properties of points B and P in Fig. 4.

The unidirectional lamina TenCate TC275-1 Epoxy Resin System was used (see Table 2) with the stacking sequence as in Eqn. (10), with $\alpha = 45°$ (point B) and $\alpha = 30°$ (point P). The cure temperature was 135° C. The natural configurations of the two resulting laminated shells are shown in Fig. 6, cf. Fig. 1a; one can hardly observe any difference in these two shapes.

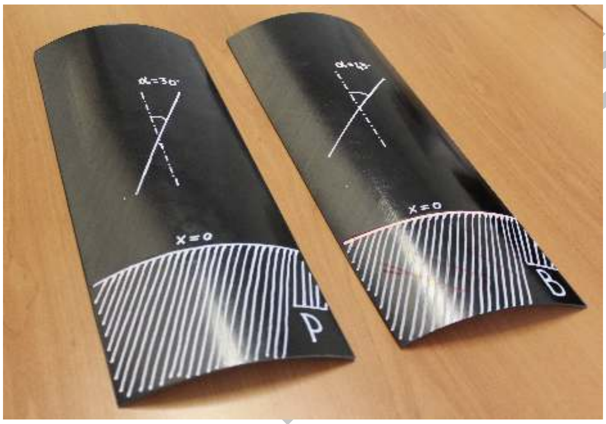

Figure 6: The laminated shells P (left) and B (right) in their natural configurations. Hatched patterns mark the regions to be clamped.

The configurations obtained after clamping the edge $x = 0$ are reported in Fig. 7. In particular, in Fig. 7a we show an overlay of the stable configurations after clamping the laminate B: the predicted shapes where shown as B_1 and B_2 in Fig. 4b.

A measure of the average axial curvature on the prototype gives $K_x \simeq 5.2\,\mathrm{m}^{-1}$; this value must to be compared with the prediction $K_x(B_2) \simeq 10.65/R \simeq 6.65\,\mathrm{m}^{-1}$ (point B_2 in Fig. 4a). The video CCshellB_alpha45.mp4, provided in the supplementary material, confirms the robustness of the bistable behavior, cfr. the energy profile $B_1 - B_2$ in Fig. 4c.

Similarly, Fig. 7b reports the shapes obtained after clamping the laminate P; this point was chosen as sensibly closer than B to the boundary of the bistability region. Whilst the lower configuration corresponds to the predicted shape P_1 in Fig. 5b and it is stable, a small force is needed to remain in the second configuration. This last shape corresponds to P_2 in Fig. 5b and was predicted to be stable but with a very small stability margin. The cause of this discrepancy is not known to the authors; small pre-stresses in the natural configuration, geometric or material imperfections could result in a small predicted stability margin to actually vanish. As a matter of fact, the boundary $E - F - G$ of the stability region in Fig. 3a is not sharp corresponding to fading stability margins of the second equilibrium branch. Keeping the maintaining force to a minimum, we have measured an average axial curvature $K_x \simeq 2.25\,\mathrm{m}^{-1}$, whilst we predicted $K_x(P_2) \simeq 4.1/R \simeq 2.55\,\mathrm{m}^{-1}$ (Point P_2 in Fig. 4a). The video CCshellP_alpha30.mp4, provided in the supplementary material, proves that the second equilibrium branch actually exists. An audible snap-through instability is indeed observed when forcing the equilibrium P_1 toward P_2 and when releasing the P_2 configuration.

(a) (b)

Figure 7: Overlay of the stable configurations for two shells shown in Fig. 6 once clamped. (a) The material refers to point B in Fig. 4a; the actual shape must be compared to B_1 and B_2 in Fig. 4b. (b) The material refers to point P in Fig. 4a; to be compared to P_1 and P_2 in Fig. 4b.

4. Conclusions

An increasing number of engineering applications exploit bistability to enhance the performance of structural systems. Focusing on the bistability of clamped shells, we have shown how the material could be tailored to achieve a variety of multistable behaviors.

In particular, we suppose our shell assembled as a composite laminate and use the polar representation [22] to parametrize the admissible domain for orthotropic elastic moduli. The advantage is to draw indications which are independent on the actual lamina used but do depend on the stacking sequence of the laminate. For two different geometries of the stress-free shell configuration, we predict the nonlinear response after one of its edges has been clamped. Imposing this boundary condition creates the stress distribution responsible for the bistable behavior. Varying the material orthotropy, the shell nonlinear response is very rich; it is characterized by different shapes of the secondary stable equilibria and by different profiles of the elastic energy content. Hence, in such structural systems, the material alone is able to determine the shapes of stable equilibria, the energetic gaps and the distance between the wells. We show that the reduced model provides such informations while simultaneously singling out their sensitivity with respect to the lamination sequences. Notably, it allows to determine the lamination angle corresponding to the desired multistable behaviour (*e.g.*, a prescribed pair of clamped stable shapes, each one with a specified robustness). In that, the model proves to be a valuable tool for design purposes, both to get preliminary indications about the design parameters and to drive FE simulations and tests on prototypes, otherwise almost useless. Clearly a simultaneous optimization of both the natural stress-free shape and the material properties could lead to a much more accurate design of the multistable structural response, but this was out of the scope of this contribution. As a matter of fact, much still remains to be done in this research field. Looking at the most promising technological applications, we deem necessary to investigate in depth both the aeroelastic behaviour and the dynamic response of multistable shells.

Appendix A. Reduced nonlinear model and stability analysis

We detail the modelling assumptions and the reduction procedure used in the stability analyses of Sect. 3. First, we briefly recall the main assumptions of the generalized von-Kármán model, see [3], [24] for details.

Starting from a flat reference configuration, we consider shell configurations in the form:

$$\mathcal{S} = \{(x + u(x,y), y + v(x,y), w(x,y)),\ 0 \leq x \leq L_x,\ -L_y/2 \leq y \leq L_y/2\},$$

where the in-plane displacement fields u and v and the transverse displacement field w scale as: $u, v = O(\varepsilon^2)$, $w = O(\varepsilon)$, with $\varepsilon = t^2/R^2$ a small parameter, being t the thickness and R the characteristic radius of curvature of the shell[1] By assuming these scaling laws, the contributions of the in-plane and transverse displacements to the membrane strains of the surface $\mathcal{S}$ are comparable, so that we have:

$$e_x = \frac{\partial u}{\partial x} + \frac{1}{2}\left(\frac{\partial w}{\partial x}\right)^2, \quad e_y = \frac{\partial v}{\partial y} + \frac{1}{2}\left(\frac{\partial w}{\partial y}\right)^2, \quad e_{xy} = \frac{1}{2}\left(\frac{\partial v}{\partial x} + \frac{\partial u}{\partial y} + \frac{\partial w}{\partial x}\frac{\partial w}{\partial y}\right), \tag{A.1}$$

while the curvatures of the surface $\mathcal{S}$ only depend on the transverse displacement:

$$k_x = \frac{\partial^2 w}{\partial x^2}, \qquad k_y = \frac{\partial^2 w}{\partial y^2}, \qquad k_{xy} = \frac{\partial^2 w}{\partial x \partial y}. \tag{A.2}$$

The stable equilibria are the local minima of the total energy $\mathcal{E}(u, v, w)$, sum of the bending and membrane contribution:

$$\mathcal{E}(u, v, w) = \frac{1}{2}\int_0^{L_x}\int_{-L_y/2}^{L_y/2} (m_x k_x + m_y k_y + m_s k_s + n_x e_x + n_y e_y + n_s e_s)\, \mathrm{d}A, \tag{A.3}$$

with the bending moments and membrane stresses as in (2).

Necessary conditions for the functional $\mathcal{E}$ to be stationary with respect to u and v are the in-plane equilibrium equations:

$$\frac{\partial n_x}{\partial x} + \frac{\partial n_s}{\partial y} = 0, \qquad \frac{\partial n_s}{\partial y} + \frac{\partial n_y}{\partial y} = 0, \tag{A.4}$$

while for the system (A.1) and (A.2) to be integrable, the Gauss compatibility condition must hold true:

$$\frac{\partial^2 e_x}{\partial y^2} + \frac{\partial^2 e_y}{\partial x^2} - 2\frac{\partial^2 e_{xy}}{\partial x \partial y} = k_x k_y - k_{xy}^2. \tag{A.5}$$

By inversion of the constitutive relations (2) and using (3), (A.5) is transformed in terms of membranal stresses to get

$$\begin{aligned} \frac{1}{t\,a\,(\beta - \nu^2)}\left[(\beta - \nu)\frac{\partial^2 n_x}{\partial y^2} + (1 - \nu)\frac{\partial^2 n_y}{\partial x^2} - \frac{(\beta - \nu^2)}{\gamma}\frac{\partial^2 n_s}{\partial x \partial y}\right] = \\ = k_x k_y - k_{xy}^2 - \frac{\partial^2 f_x}{\partial y^2} - \frac{\partial^2 f_y}{\partial x^2} + 2\frac{\partial^2 f_{xy}}{\partial x \partial y} = \det \boldsymbol{k} - \det \boldsymbol{h}. \end{aligned} \tag{A.6}$$

where $\boldsymbol{h}$ denotes the curvature of the shell natural configuration. Equations (A.4) and (A.6) constitute a linear system of differential equations to compute the membrane stresses in term of the curvature field $\boldsymbol{k}$. In what follow we exploits this fact to deduce a discrete approximation of the energy functional (A.3), see [24] or [1] for more details.

Step 1. We seek for displacement fields w in the form

$$w(x, y) = q_1\frac{x^2}{2} + q_2\frac{y^2}{2} + q_3\frac{x^3}{6} + q_4\frac{x^2 y^2}{2} + q_5\frac{x y^2}{2}, \tag{A.7}$$

uniquely defined by five Lagrangian parameters, q_1 to q_5. Such an ansatz covers the assumption (A.7) and allows us to clamp the shell on the edge $x = 0$ by fixing $q_2 = 0$ and $q_5 = 0$.

[1] With $t = 1$ mm and $R \simeq 1.61\,\mathrm{m}$, the curvatures in Table 1, the shell shallowness is evaluated to be $\varepsilon = t^2/R^2 \simeq 10^{-4}$.

Step 2. Using (A.2), the forcing term in (A.6) is evaluated to be

$$\det \boldsymbol{k} - \det \boldsymbol{h} = q_1 q_4\, x^2 + q_3 q_4\, x^3 - 3\, q_4^2\, x^2\, y^2 + \frac{(h_1 - h_2)^2}{L_x^2}\, y^2. \tag{A.8}$$

Here, according to Eqn. (1), $\det \boldsymbol{h} = -(h_1 - h_2)^2 y^2 / L_x^2$.

Step 3. After introducing (A.8) into (A.6), we use a standard finite-element code to solve the membrane problem (A.4)-(A.6) with respect to the Lagrangian parameters q_1, q_3 and q_4. A high numerical precision to estimate the membranal stresses ensures a good estimate of the membrane energy, which is the dominant term of the elastic energy functional.

Step 4. Inserting the ansatz (A.7) and the computed membrane stresses in (A.3) we finally obtain a reduced energy funtional $\mathcal{E} = \bar{\mathcal{E}}(\boldsymbol{q})$, which is a fourth-order polynomial in the Lagrangian parameters $\boldsymbol{q} = (q_1, q_3, q_4)$.

We prefer the minimization of the reduced energy $\bar{\mathcal{E}}(\boldsymbol{q})$ to a standard finite-element discretization of the original energy functional (A.3). Indeed, in order to find all the branches of the shell equilibria, we could rely on polynomial root-finding techniques of the system $\partial \bar{\mathcal{E}} / \partial \boldsymbol{q} = \boldsymbol{0}$. These techniques become computationally infeasible when the number of degrees of freedom becomes large.

Appendix B. Optimal path between minima

Once a bistable shell is given, the estimate of the energetic gaps between the two stable equilibria is a question of relevant importance. To this aim, we sketch below a procedure to compute, in the space of Lagrangian parameters, an optimal trajectory connecting the two minima. Specifically, a trajectory is said to be optimal if it minimizes the maximum value attained by the elastic energy. This is pictorially equivalent to finding a "mountain pass" between two valleys; once the height of the pass is found the two energetic gaps are clearly defined.

For assigned material parameters we suppose to be given an energy functional $\bar{\mathcal{E}}(\boldsymbol{q})$ characterized by two distinct minima, say $\boldsymbol{q}_a$ and $\boldsymbol{q}_b$. For every smooth curve $s \in [0,1] \mapsto \boldsymbol{q}(s)$ connecting the two minima, *i.e.* $\boldsymbol{q}(0) = \boldsymbol{q}_a$, and $\boldsymbol{q}(1) = \boldsymbol{q}_b$, we define the "smoothing" functional

$$S(\boldsymbol{q}(\cdot)) = \int_0^1 \|\boldsymbol{q}''(s)\|^2\, ds + \Big(\max_s \|\boldsymbol{q}'\| - \min_s \|\boldsymbol{q}'\| \Big)^2, \tag{B.1}$$

and the "maximal-energy" functional

$$E(\boldsymbol{q}(\cdot)) = \max_{s \in [0,1]} \bar{\mathcal{E}}(\boldsymbol{q}(s)). \tag{B.2}$$

Starting from $k = 0$, we iteratively solve, until convergence, the minimization problem

$$\boldsymbol{q}^{k+1} = \mathrm{argmin}_{\boldsymbol{q}} \left[S(\boldsymbol{q}(\cdot)) + c\, k\, E(\boldsymbol{q}(\cdot)) \right], \quad c > 0, \quad k = 0, 1, 2, ... \tag{B.3}$$

using as a tentative solution the curve $\boldsymbol{q}^k$.

We note that in the first iteration, $k = 0$, the resulting optimal trajectory is the straight line between the minima $\boldsymbol{q}^0(s) = (1 - s)\, \boldsymbol{q}_a - s\, \boldsymbol{q}_b$ (depicted in red in Fig. B.8). Clearly, as $S(\boldsymbol{q}^0) = 0$, the global minimum is reached. However, as k increases, the maximal-energy functional E in (B.2) enters the game, since its relative cost with respect to the smoothing functional increases. The real value c is used to control such cost. For $k > 0$ the straight path is not any more optimal and the path is distorted in order to achieve a lower value of the energy gap. In Fig. B.8a we have plotted, in a three-dimensional Lagrangian space $\boldsymbol{q} = (q_1, q_3, q_4)$, the energy level sets for a bistable shell; in the same figure the first iterate $\boldsymbol{q}^0(s)$, the intermediate steps and the final optimal path $\boldsymbol{q}^{\bar{k}}(s)$ are shown by a red straight line, a set of grey curves and a thick black curve respectively. Fig. B.8b reports the elastic energy values on such trajectories.

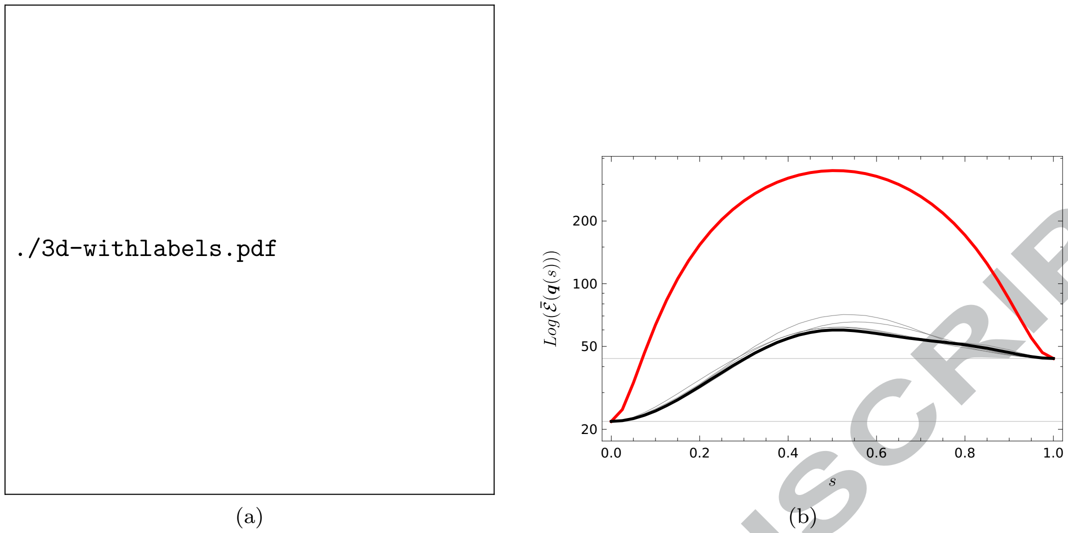

Figure B.8: a) Level sets for the elastic energy of a bistable shell and the straight (red) and optimized (black) paths between the two minima. Intermediate steps, for $0 < k < \bar{k}$ in (B.3), are reported as thin grey curves. b) Logarithmic plot of the energy along this paths.

Acknowledgement

The authors acknowledge the financial support of Project ANR-13-JS09-0009 (Agence Nationale de la Recherche, France).

References

[1] M Brunetti, A Vincenti and S Vidoli. A class of morphing shell structures satisfying clamped boundary conditions. *Int. Journal of Solids & Structures*, 82:47 – 55, 2016

[2] J Berthelot. Materials. Mechanical Behavior and Structural Analysis. Springer, 1999

[3] P G Ciarlet. A justification of the von Kármán equations. *Archive for Rational Mechanics and Analysis*, 73:349–389, 1980

[4] B H Coburn, A Pirrera, P M Weaver, and S Vidoli. Tristability of an orthotropic doubly curved shell. *Composite Structures*, 96:446–454, 2013

[5] S Daynes, P M Weaver, and J A Trevarthen. A morphing composite air inlet with multiple stable shapes. *Journal of Intelligent Material Systems and Structures*, 22(9):961–973, 2011

[6] A Fernandes, C Maurini, and S Vidoli. Multiparameter actuation for shape control of bistable composite plates. *Int. Journal of Solids & Structures*, 47(10):1449–1458, 2010

[7] E Lamacchia, A Pirrera, I V Chenchiah, and P M Weaver. Morphing shell structures: A generalised modelling approach. *Composite Structures*, 131:1017-1027, 2015

[8] F Mattioni, P M Weaver and M I Friswell. Multistable composite plates with piecewise variation of lay-up in the planform. *Int. Journal of Solids & Structures*, 46(1):151-164, 2009

[9] W Hamouche, C Maurini, A Vincenti, and S Vidoli. Simple recipes to design and produce multistable shells. *Meccanica*, 51: 2305-2320, 2016

[10] M Montemurro, A Vincenti and P Vannucci. Design of the elastic properties of laminates with a minimum number of plies. *Mechanics of Composite Materials*, 48(4):369 – 390, 2012

[11] W Hamouche, C Maurini, S Vidoli, A Vincenti. *Multi-parameter actuation of a neutrally stable shell: a flexible gear-less motor. Proceedings Royal Society of London A*, 473 (2204), 2017

[12] M Montemurro, A Vincenti and P Vannucci. A Two-Level Procedure for the Global Optimum Design of Composite Modular Structures. J*ournal of Optimization Theory and Applications*, 155(1), 1 − 23, 2012

[13] A D Norman, K A Seffen, and S D Guest. Multistable corrugated shells. *Proceedings of the Royal Society of London A*, 464(2095), 1653-1672, 2008

[14] A S Panesar and P M Weaver. Optimisation of blended bistable laminates for a morphing flap. *Composite Structures*, 94(10), 3092-3105, 2012

[15] A Pirrera, D Avitabile, and P M Weaver. On the thermally induced bistability of composite cylindrical shells for morphing structures. *Int. Journal of Solids & Structures*, 49(5), 685–700, 2012

[16] S Chiacchiari, F Romeo, DM McFarland, LA Bergman, AF Vakakis. Vibration energy harvesting from impulsive excitations via a bistable nonlinear attachment *Int. Journal of Non-Linear Mechanics*, 94: 84-97, 2017

[17] K A Seffen. Morphing bistable orthotropic elliptical shallow shells. *Proceedings of the Royal Society A*, 463(2077), 67–83, 2007

[18] S W Tsai and T Hahn. Introduction to composite materials. *Technomic*, 1980

[19] P Vannucci and G Verchery. A special class of uncoupled and quasi-homogeneous laminates. *Composites Science and Technology*, 61(10), 1465 − 1473, 2001

[20] P Vannucci. Plane anisotropy by the polar method. *Meccanica*, 40(4-6), 437 − 454, 2005

[21] P Vannucci. A note on the elastic and geometric bounds for composite laminates. *Journal of Elasticity*, 112(2), 199 − 215, 2013

[22] G Verchery. Les invariants des tenseurs d'ordre 4 du type de l'elasticitè. *Mechanical Behavior of Anisotropic Solids*, 93 − 104, 1982

[23] S Vidoli and C Maurini. Tristability of thin orthotropic shells with uniform initial curvature. *Proceedings of the Royal Society A*, 464(2099), 2949–2966, 2008

[24] S Vidoli. Discrete approximations of the Föppl - von Kármán shell model: From coarse to more refined models. *Int. Journal of Solids & Structures*, 50(9), 1241 − 1252, 2013

[25] T Von Kármán. *Festigkeitsprobleme im maschinenbau.* Encyklopädie der Mathematischen Wissenschaften. 1910

[26] Aviorec S.R.L. *http://www.aviorec.com*

[27] Tencate TC275-1 Datasheet. *https://www.tencatecomposites.com/product-explorer/products/hKxc/TC275-1*